AAS 21-368

INDIRECT OPTIMIZATION FOR LOW-THRUST TRANSFERS WITH EARTH-SHADOW ECLIPSES

Yang Wang*, Francesco Topputo†

An efficient indirect method is presented to solve optimal low-thrust Earth-orbit transfers in presence of shadow eclipses. The key feature of our method is the capability to offer accurate gradients of problem functions with respect to all decision variables, which is pivotal for robust convergence. Particular attention is paid to handling the discontinuity conduced by Earth-shadow eclipses. The state transition matrix at shadow entrance and exit is compensated based on calculus of variations. A systematic framework for solving both time-optimal and fuel-optimal problems is established by combining analytic derivatives, switching time detection and two-level continuation with an augmented integration flowchart. The GTO to GEO transfers are simulated to illustrate the effectiveness and efficiency of the method developed.

INTRODUCTION

The solar electric propulsion (SEP) enables the spacecraft to maneuver with higher specific impulse and thus lower fuel consumption compared with chemical propulsion. The use of SEP as the primary propulsion attracts increasing attentions. However, the SEP-based low-thrust trajectory optimization for Earth-orbit transfers is a long-duration challenging task, because the low thrust-to-mass radio usually requires long flight time, thus large number of spirals, to complete the transfer. Moreover, the power generated from solar panels is insufficient to drive the engine when the spacecraft passes through the Earth-shadow eclipses, which makes this nonlinear optimal control problem (NOCP) harder to solve.

Typically, two types of numerical solution methods dedicated to low-thrust trajectory optimization, categorized as direct and indirect methods.[1] Developing a robust indirect method is the context of this work. Through transforming the NOCP to a two-point boundary value problem (TPBVP) by first-order necessary conditions of optimality, indirect methods further solve the TPBVP as a zero-finding problem, the solution of which is guaranteed to be a least extremal.[2] However, few works were dedicated to solving low-thrust optimization with Earth-shadow eclipses using indirect methods. Ferrier and Epenoy[3] showed that Earth-shadow constraints cannot be treated by classical Pontryagin's principle directly, and proposed to smooth the thrust modulus during shadow entrance and exit to avoid the discontinuity. Cerf[4] treated the Earth-shadow constraint as an interior-point constraint, and solved the minimum-time transfer with Cartesian coordinate dynamics. Geffroy

*PhD candidate, Department of Aerospace Science and Technology, Politecnico di Milano, Via La Masa 34, Milano, Italy, 20156. E-mail address: yang.wang@polimi.it.

†Associate Professor, Department of Aerospace Science and Technology, Politecnico di Milano, Via La Masa 34, Milano, Italy, 20156. E-mail address: francesco.topputo@polimi.it.

and Epenoy[5] developed the average technique into indirect optimization, and solved nearly time-optimal solution in the presence of Earth-shadow eclipses. Recently, Woollands and Taheri[6] presented hyperbolic tangent smoothing technique, which gradually approaches fuel-optimal solutions with broader convergence domain.

This work presents a robust indirect method featuring accurate gradients for low-thrust trajectory optimization considering Earth-shadow eclipses. The gradients are computed through the state transition matrix (STM) and the chain rule, where STM across discontinuity is compensated based on calculus of variations. The integration flowchart in Zhang et al.[7] is augmented to involve event branches of shadow entrance and exit. In order to alleviate the numerical difficulty caused by discontinuity, two-level continuation is designed. The first level continues from the time-optimal and energy-optimal solutions without shadow constraints to the solutions with shadow constraints. The second level continues from the energy-optimal solution to the fuel-optimal solution. The solver framework is established by combining analytic derivatives, continuation and switching detection technique with the augmented integration flowchart. Both the time-optimal and fuel-optimal solutions with accurate bang-bang control can be obtained without prescribing the bang-bang control structure a priori. The GTO to GEO transfers are investigated to illustrate the effectiveness and efficiency of the method developed.

The rest of the paper proceeds as follows. Section II presents dynamical equations of modified equinoctial elements, the geometrical model of Earth-shadow eclipses and optimal control problem statement. Section III depicts the indirect method developed. In Section IV, simulations are presented for the GTO to GEO transfers. Finally, Section V concludes the paper.

PROBLEM STATEMENT

Dynamical equations

The modified equinoctial elements (MEE) are used to describe the orbital dynamics of spacecraft since MEE are non-singular orbital elements and well behaved during one revolution[8] . The relationship between MEE and classical orbital elements is

$$\begin{aligned} p &= a(1-e^2) \\ e_x &= e\cos(\omega+\Omega) \\ e_y &= e\sin(\omega+\Omega) \\ h_x &= \tan(i/2)\cos\Omega \\ h_y &= \tan(i/2)\sin\Omega \\ L &= \omega+\Omega+\theta \end{aligned} \tag{1}$$

where a is the semi-major axis, e is the eccentricity, i is the orbital inclination, Ω is the right ascension of the ascending node, ω is the argument of perigee, θ is the true anomaly, p is the semilatus rectum and L is the true longitude. Denote the MEE vector as $\boldsymbol{x}_{\rm mee} = [p, e_x, e_y, h_x, h_y, L]^\top$ and the state vector as $\boldsymbol{x} = [\boldsymbol{x}_{\rm mee}, m]$ where m is the mass variable, equations of motion of the spacecraft are

$$\dot{\boldsymbol{x}} = \boldsymbol{f}(t, \boldsymbol{x}, \boldsymbol{\alpha}, u) \Rightarrow \begin{pmatrix} \dot{\boldsymbol{x}}_{\rm mee} \\ \dot{m} \end{pmatrix} = \begin{pmatrix} u\,\dfrac{T_{\max}}{m}\,\boldsymbol{B}\,\boldsymbol{\alpha} + \boldsymbol{A} \\ -\dfrac{T_{\max}}{c}\,u \end{pmatrix} \tag{2}$$

where $u \in [0,1]$ is the thrust throttle, $\boldsymbol{\alpha}$ is the thrust pointing direction, $c = I_{\rm sp} g_0$ is the exhaust velocity, $I_{\rm sp}$ is the specific impulse, g_0 is the gravity acceleration at sea level and $T_{\max}$ is the maximum thrust magnitude. $I_{\rm sp}$ and $T_{\max}$ are assumed constant during the flight. In Eq. (2),

$$\boldsymbol{A} = [0,0,0,0,0,\kappa]^\top \tag{3}$$

$$\boldsymbol{B} = \begin{bmatrix} 0 & \frac{2p}{\nu}\sqrt{\frac{p}{\mu}} & 0 \\ \sqrt{\frac{p}{\mu}}\sin L & \sqrt{\frac{p}{\mu}}[(\nu+1)\cos L + e_x]\frac{1}{\nu} & -\sqrt{\frac{p}{\mu}}[h_x \sin L - h_y \cos L]\frac{e_y}{\nu} \\ -\sqrt{\frac{p}{\mu}}\cos L & \sqrt{\frac{p}{\mu}}[(\nu+1)\sin L + e_y]\frac{1}{\nu} & \sqrt{\frac{p}{\mu}}[h_x \sin L - h_y \cos L]\frac{e_x}{\nu} \\ 0 & 0 & \sqrt{\frac{p}{\mu}}\frac{s^2}{2\nu}\cos L \\ 0 & 0 & \sqrt{\frac{p}{\mu}}\frac{s^2}{2\nu}\sin L \\ 0 & 0 & \frac{1}{\nu}\sqrt{\frac{p}{\mu}}(h_x \sin L - h_y \cos L) \end{bmatrix} \tag{4}$$

where μ is the gravitational parameter and

$$\nu = 1 + e_x \cos L + e_y \sin L, \quad s^2 = 1 + h_x^2 + h_y^2, \quad \kappa = \sqrt{\mu p}\left(\frac{\nu}{p}\right)^2 \tag{5}$$

The boundary conditions are

$$\begin{gathered} p(t_0) = p_0, \quad e_x(t_0) = e_{x0}, \quad e_y(t_0) = e_{y0}, \\ h_x(t_0) = h_{x0}, \quad h_y(t_0) = h_{y0}, \quad L(t_0) = L_0, \quad m(t_0) = m_0 \\ p(t_f) = p_f, \quad e_x(t_f) = e_{xf}, \quad e_y(t_f) = e_{yf}, \\ h_x(t_f) = h_{xf}, \quad h_y(t_f) = h_{yf}, \quad L(t_f) = \text{free}, \quad m(t_f) = \text{free} \end{gathered} \tag{6}$$

The MEE elements are related to the Cartisian coordinate $(\boldsymbol{r}, \boldsymbol{v})$ through

$$\boldsymbol{r} = \begin{bmatrix} \frac{p}{s^2\nu}\left(\cos L + \alpha^2 \cos L + 2h_x h_y \sin L\right) \\ \frac{p}{s^2\nu}\left(\sin L - \alpha^2 \sin L + 2h_x h_y \cos L\right) \\ \frac{2p}{s^2\nu}\left(h_x \sin L - h_y \cos L\right) \end{bmatrix} \tag{7}$$

$$\boldsymbol{v} = \begin{bmatrix} -\frac{1}{s^2}\sqrt{\frac{\mu}{p}}\left(\sin L + \alpha^2 \sin L - 2h_x h_y \cos L + e_y - 2e_x h_x h_y + \alpha^2 e_y\right) \\ -\frac{1}{s^2}\sqrt{\frac{\mu}{p}}\left(-\cos L + \alpha^2 \cos L + 2h_x h_y \sin L - e_x + 2e_y h_x h_y + \alpha^2 e_x\right) \\ \frac{2}{s^2}\sqrt{\frac{\mu}{p}}\left(h_x \cos L + h_y \sin L + e_x h_x + e_y h_y\right) \end{bmatrix} \tag{8}$$

where

$$\alpha^2 = h_x^2 - h_y^2 \tag{9}$$

Earth-shadow eclipses

Two geometric shadow models, i.e., cylindrical model[3,4,6] and cone model,[9,10] are mainly used in literature. The cone model is adopted since it is more practical and accurate. When the spacecraft passes through the umbra shadow, the solar energy is completely lost, while limited solar energy is received when the spacecraft locates in the penumbra shadow. For simplicity, the engine switches off when the spacecraft passes through either umbra or penumbra shadow. Since umbra shadow is a portion of the penumbra shadow,[10] only penumbra geometry in Fig. 1 is discussed.

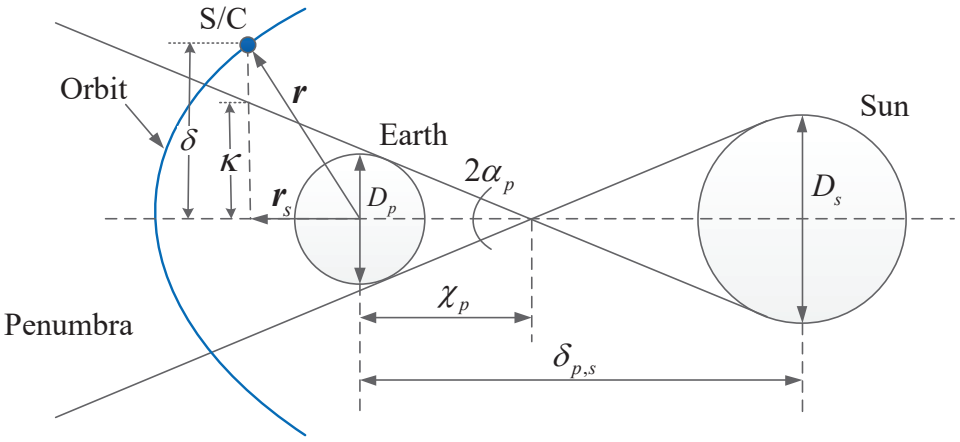

Figure 1: The geometry of penumbra shadow.

In order to simplify the penumbra shadow model, several assumptions are made. Firstly, both the Sun and the Earth are assumed spherical bodies, thus the penumbra shadow is conical projections. Secondly, the Earth orbit is assumed planar and circular with respect to the Sun. Based on these assumptions, the solar unit vector $\hat{\boldsymbol{s}}$ is analytical. In the ecliptic coordinate, the Sun-Earth angle is approximated as $\theta_s = \theta_{s,0} + n(t - t_0)$, where $\theta_{s,0}$ is the initial Sun-Earth angle at t_0 and $n = 360^\circ/365.25$. The solar unit vector under ecliptic coordinate is $\hat{\boldsymbol{s}}_{\text{ec}} = [\cos\theta_s, \sin\theta_s, 0]^\top$. Transforming $\hat{\boldsymbol{s}}_{\text{ec}}$ to equatorial coordinate, there satisfies $\hat{\boldsymbol{s}} = [\cos(\theta_s), \cos(i_e)\sin(\theta_s), \sin(i_e)\sin(\theta_s)]$, where $i_e = 23.26^\circ$ is the ecliptic obliquity.

In Fig. 1, D_p and D_s are diameters of the Earth and the Sun, $\delta_{p,s}$ is the distance between them, and χ_p satisfies

$$\chi_p = \frac{D_p\,\delta_{p,s}}{D_s + D_p} \tag{10}$$

The angle α_p is

$$\alpha_p = \sin^{-1}\frac{D_p}{2\chi_p} \tag{11}$$

The projection of the spacecraft position vector on the solar unit position vector is

$$\boldsymbol{r}_s = (\boldsymbol{r}\cdot\hat{\boldsymbol{s}})\hat{\boldsymbol{s}} \tag{12}$$

The vertical vector between the center of the penumbra cone and the spacecraft is

$$\boldsymbol{\delta} = \boldsymbol{r} - \boldsymbol{r}_s \tag{13}$$

The distance between the center of the penumbra cone and the penumbra terminator point at the projected spacecraft location is

$$\kappa = (\chi_p + \|\boldsymbol{r}_s\|) \tan \alpha_p \tag{14}$$

The comparison of the magnitude of the vector $\boldsymbol{\delta}$ with the distance κ, i.e.,

$$S_d(t, \boldsymbol{r}) = \|\boldsymbol{\delta}\| - \kappa \tag{15}$$

is introduced as the manually defined shadow switching function. The conditions for the spacecraft to enter or exit the shadow are

- Penumbra terminator points are only feasible if $\boldsymbol{r} \cdot \hat{\boldsymbol{s}} < 0$.
- Penumbra terminator points occur when $S_d = 0$, and the spacecraft is in the penumbra cone if $S_d < 0$.

For easy discussion below, a signal variable p_{type} is defined to label the position of the spacecraft with respect to the shadow region, as

$$p_{\text{type}} = \begin{cases} \text{in}, & \text{if} \quad S_d < 0 \quad \text{and} \quad \boldsymbol{r} \cdot \hat{\boldsymbol{s}} < 0 \\ \text{out}, & \text{if} \quad \text{otherwise} \end{cases} \tag{16}$$

Fuel-optimal problem

The performance index of the fuel-optimal (FO) problem is

$$J_f = \frac{T_{\max}}{c} \int_{t_0}^{t_f} u \, \mathrm{d}t \tag{17}$$

where t_0 and t_f are fixed initial and terminal time instants. In the FO problem, the optimal thrust throttle u^* profile reveals the bang-bang control structure.[8] In order to alleviate the numerical difficulty, a continuation technique[7] is employed. The strategy is to solve energy-optimal (EO) problem ($\varepsilon = 1$) first, and continues the solution manifold while gradually reducing the manually embedded parameter ε, until the solution to the FO problem ($\varepsilon = 0$) is found. The performance index of the energy-to-fuel-optimal (EO2FO) problem is

$$J_\varepsilon = \frac{T_{\max}}{c} \int_{t_0}^{t_f} [u - \varepsilon u(1-u)] \, \mathrm{d}t \tag{18}$$

The Hamiltonian function reads

$$H_\varepsilon = \frac{T_{\max}}{c} [u - \varepsilon u(1-u)] + \lambda_L \kappa + u \frac{T_{\max}}{m} \boldsymbol{\lambda}_{\text{mee}}^\top \boldsymbol{B} \, \boldsymbol{\alpha} - \lambda_m \, u \frac{T_{\max}}{c} \tag{19}$$

where $\boldsymbol{\lambda} = [\boldsymbol{\lambda}_{\text{mee}}, \lambda_m]$ is the costate vector associate with $\boldsymbol{x}$. By virtue of the Pontryagin minimum principle (PMP),[2] the optimal thrust direction satisfies

$$\boldsymbol{\alpha}^* = -\frac{\boldsymbol{B}^\top \boldsymbol{\lambda}_{\text{mee}}}{\|\boldsymbol{B}^\top \boldsymbol{\lambda}_{\text{mee}}\|} \tag{20}$$

Substituting $\boldsymbol{\alpha}^*$ into Hamiltonian function Eq. (19) yields

$$H_\varepsilon = \lambda_L \kappa + u \frac{T_{\max}}{c} \left[S_\varepsilon - \varepsilon(1-u) \right] \tag{21}$$

where the throttle switching function S_ε is

$$S_\varepsilon = -\frac{c}{m} \| \boldsymbol{B}^\top \boldsymbol{\lambda}_{\text{mee}} \| - \lambda_m + 1 \tag{22}$$

The optimal thrust throttle u^* is determined by PMP and the Earth-shadow constraint as

$$u^* = \begin{cases} 0, & \text{if} \quad S_\varepsilon > \varepsilon \quad \text{or} \quad p_{\text{type}} = \text{in} \\ (\varepsilon - S_\varepsilon)/2\varepsilon & \text{if} \quad -\varepsilon < S_\varepsilon < \varepsilon \quad \text{and} \quad p_{\text{type}} = \text{out} \\ 1, & \text{if} \quad S_\varepsilon < -\varepsilon \quad \text{and} \quad p_{\text{type}} = \text{out} \end{cases} \tag{23}$$

Note that an interior-point constraint should be addressed to ensure that Eq. (23) satisfies necessary conditions of optimality, which will be discussed later.

Let $\boldsymbol{y} \coloneqq [\boldsymbol{x}, \boldsymbol{\lambda}] \in \mathbb{R}^{14}$ be the collection of state and costate vector, the motion of the spacecraft is determined by integrating the following dynamics

$$\dot{\boldsymbol{y}} = \boldsymbol{F}(t, \boldsymbol{y}, u, \boldsymbol{\alpha}) \Rightarrow \begin{cases} \dot{\boldsymbol{x}}_{\text{mee}} & = \left[\dfrac{\partial H_\varepsilon}{\partial \boldsymbol{\lambda}_{\text{mee}}} \right]^\top = u \, \dfrac{T_{\max}}{m} \, \boldsymbol{B} \, \boldsymbol{\alpha} + \boldsymbol{A} \\ \dot{m} & = \dfrac{\partial H_\varepsilon}{\partial \lambda_m} = -\dfrac{T_{\max}}{c} \, u \\ \dot{\boldsymbol{\lambda}}_{\text{mee}} & = -\left[\dfrac{\partial H_\varepsilon}{\partial \boldsymbol{x}_{\text{mee}}} \right]^\top = -\lambda_L \left[\dfrac{\partial \kappa}{\partial \boldsymbol{x}_{\text{mee}}} \right]^\top - u \, \dfrac{T_{\max}}{m} \left[\dfrac{\partial \boldsymbol{B}^\top \boldsymbol{\lambda}_{\text{mee}}}{\partial \boldsymbol{x}_{\text{mee}}} \right]^\top \boldsymbol{\alpha} \\ \dot{\lambda}_m & = -\dfrac{\partial H_\varepsilon}{\partial m} = u \, \dfrac{T_{\max}}{m^2} \boldsymbol{\lambda}_{\text{mee}}^\top \boldsymbol{B} \boldsymbol{\alpha} \end{cases} \tag{24}$$

Since the terminal true longitude and mass are free, there exists

$$\lambda_L(t_f) = 0, \quad \lambda_m(t_f) = 0 \tag{25}$$

Remark 1 *Let $\boldsymbol{y}(t) = \boldsymbol{\varphi}_\varepsilon([\boldsymbol{x}_0, \boldsymbol{\lambda}_0], t_0, t)$ be the solution flow integrated Eq.* (24) *from the initial time t_0 to the generic time t, using the optimal control u^* in Eq.* (23) *and $\boldsymbol{\alpha}^*$ in Eq.* (20)*. The EO2FO problem is to find $\boldsymbol{\lambda}_0^*$ such that $\boldsymbol{y}(t_f) = \boldsymbol{\varphi}_\varepsilon([\boldsymbol{x}_0, \boldsymbol{\lambda}_0^*], t_0, t_f)$ satisfies Eqs.* (6) *and* (25)*.*

Time-optimal problem

The performance index of the time-optimal (TO) problem is

$$J_t = \int_{t_0}^{t_f} 1 \mathrm{d}t \tag{26}$$

where t_f in this case is free.

The Hamiltonian function reads

$$H_t = 1 + \lambda_L \kappa + u \, \frac{T_{\max}}{m} \, \boldsymbol{\lambda}_{\text{mee}}^\top \, \boldsymbol{B} \, \boldsymbol{\alpha} - \lambda_m \, u \, \frac{T_{\max}}{c} \tag{27}$$

The optimal thrust angle $\boldsymbol{\alpha}^*$ is the same as Eq. (20). Substituting Eq. (20) into Eq. (27) yields

$$H_t = 1 + \lambda_L \kappa + u \frac{T_{\max}}{c} S_t \tag{28}$$

where the throttle switching function S_t is

$$S_t = -\frac{c}{m} \| \boldsymbol{B}^\top \boldsymbol{\lambda}_{\mathrm{mee}} \| - \lambda_m \tag{29}$$

The optimal thrust throttle u^* is determined by PMP and the Earth-shadow constraint as

$$u^* = \begin{cases} 0, & \text{if} \quad p_{\mathrm{type}} = \mathrm{in} \\ 1, & \text{if} \quad p_{\mathrm{type}} = \mathrm{out} \end{cases} \tag{30}$$

The transversality condition at terminal time t_f is

$$H_t(t_f) = 0 \tag{31}$$

Remark 2 *The dynamics for the TO problem is the same as Eq.* (24)*. Let* $\boldsymbol{y}(t) = \boldsymbol{\varphi}_t([\boldsymbol{x}_0, \boldsymbol{\lambda}_0], t_0, t)$ *be the solution flow integrated Eq.* (24) *from the initial time* t_0 *to the generic time* t*, using the optimal control* u^* *in Eq.* (30) *and* $\boldsymbol{\alpha}^*$ *in Eq.* (20)*. The TO problem is to find* $\boldsymbol{\lambda}_0^*$ *and* t_f^* *such that* $\boldsymbol{y}(t_f) = \boldsymbol{\varphi}_t([\boldsymbol{x}_0, \boldsymbol{\lambda}_0^*], t_0, t_f^*)$ *satisfies Eqs.* (6)*,* (25) *and* (31)*.*

Interior-point constraint

From physical reality, the SEP engine switches on/off when the spacecraft exits/enters the Earth-shadow eclipse. However, according to PMP, this operation may be not optimal. In order to satisfy the necessary conditions of optimality, the events of shadow entrance and exit should be treated as interior–point constraints.[4] Suppose that there satisfies $S_d(t_s) = 0$, and p_{type} switches between 'in' and 'out' at t_s, then[2]

$$H(t_s^-) = H(t_s^+) - \pi \frac{\partial S_d}{\partial t} \tag{32}$$

$$\boldsymbol{\lambda}_{\mathrm{mee}}^\top(t_s^-) = \boldsymbol{\lambda}_{\mathrm{mee}}^\top(t_s^+) + \pi \frac{\partial S_d}{\partial \boldsymbol{x}_{\mathrm{mee}}} \tag{33}$$

where t_s^- and t_s^+ are time instants instantaneously before and after t_s, and π is a scalar Lagrange multiplier. In Eq. (33), costate $\boldsymbol{\lambda}_{\mathrm{mee}}$ is discontinuous since S_d is the function of $\boldsymbol{x}_{\mathrm{mee}}$. It is easy to verify that

$$\frac{\partial \boldsymbol{r}}{\partial \boldsymbol{x}_{\mathrm{mee}}} \boldsymbol{B} = \boldsymbol{0}_{3\times 3} \tag{34}$$

Then we have

$$\boldsymbol{B}^\top \boldsymbol{\lambda}_{\mathrm{mee}}(t_s^+) = \boldsymbol{B}^\top \left[\boldsymbol{\lambda}_{\mathrm{mee}}(t_s^-) - \pi \left(\frac{\partial S_d}{\partial \boldsymbol{x}_{\mathrm{mee}}} \right)^\top \right] = \boldsymbol{B}^\top \boldsymbol{\lambda}_{\mathrm{mee}}(t_s^-) \tag{35}$$

Thus the thrust angle $\boldsymbol{\alpha}^*$ in Eq. (20), throttle switching functions S_ε in Eq. (22) and S_t in Eq. (29) are continuous across t_s. The time derivative of S_d is simplified as

$$\dot{S}_d = \frac{\partial S_d}{\partial \boldsymbol{x}_{\mathrm{mee}}} \left(\boldsymbol{A} + u \frac{T_{\max}}{m} \boldsymbol{B}\boldsymbol{\alpha} \right) + \frac{\partial S_d}{\partial t} = \frac{\partial S_d}{\partial L} \kappa + \frac{\partial S_d}{\partial t} \tag{36}$$

Let π_t and π_ε be the π variables for the TO and EO2FO problems, respectively, the discussions are elaborated below.

1) For the TO problem, the Hamiltonian functions at t_s^- and t_s^+ are

$$H_t(t_s^-) = \lambda_L(t_s^-)\kappa + u(t_s^-)\frac{T_{\max}}{c}\,S_t + 1 \tag{37}$$

$$H_t(t_s^+) = \lambda_L(t_s^+)\kappa + u(t_s^+)\frac{T_{\max}}{c}\,S_t + 1 \tag{38}$$

Combining Eqs. (32), (33), (37) and (38) yields

$$\pi_t = \Delta u \frac{T_{\max}}{c}\frac{S_t}{\dot{S}_d} \tag{39}$$

where $\Delta u = u(t_s^+) - u(t_s^-)$. Then $\boldsymbol{\lambda}_{\text{mee}}(t_s^+)$ is calculated as

$$\boldsymbol{\lambda}_{\text{mee}}^\top(t_s^+) = \boldsymbol{\lambda}_{\text{mee}}^\top(t_s^-) - \pi_t \frac{\partial S_d}{\partial \boldsymbol{x}_{\text{mee}}} \tag{40}$$

2) For the EO2FO problem, the Hamiltonian functions at t_s^- and t_s^+ are

$$H_\varepsilon(t_s^-) = \lambda_L(t_s^-)\kappa + u(t_s^-)\frac{T_{\max}}{c}\left(S_\varepsilon - \varepsilon + \varepsilon u(t_s^-)\right) \tag{41}$$

$$H_\varepsilon(t_s^+) = \lambda_L(t_s^+)\kappa + u(t_s^+)\frac{T_{\max}}{c}\left(S_\varepsilon - \varepsilon + \varepsilon u(t_s^+)\right) \tag{42}$$

Combining Eq. (32), (33), (36), (41) and (42) yields

$$\pi_\varepsilon = \Delta u \frac{T_{\max}}{c}\frac{S_\varepsilon - \varepsilon + (u(t_s^+) + u(t_s^-))\varepsilon}{\dot{S}_d} \tag{43}$$

Then $\boldsymbol{\lambda}_{\text{mee}}(t_s^+)$ is calculated as

$$\boldsymbol{\lambda}_{\text{mee}}^\top(t_s^+) = \boldsymbol{\lambda}_{\text{mee}}^\top(t_s^-) - \pi_\varepsilon \frac{\partial S_d}{\partial \boldsymbol{x}_{\text{mee}}} \tag{44}$$

INDIRECT METHOD

Analytic derivative

The analytical gradients are computed through state transition matrix (STM) and the chain rule. The STM maps small variations in the initial conditions $\delta \boldsymbol{y}_0$ over $t_0 \to t$, i.e., $\delta \boldsymbol{y} = \Phi(t_0, t)\delta \boldsymbol{y}(t_0)$. STM subjects to

$$\dot{\Phi}(t_0, t) = D_y \boldsymbol{F}\, \Phi(t_0, t) \tag{45}$$

where $D_y \boldsymbol{F}$ is the derivative of dynamical equations Eq. (24) w.r.t. $\boldsymbol{y}$, and $\Phi(t_0, t_0) = I_{14\times 14}$.

Let $\boldsymbol{z} \coloneqq [\boldsymbol{y}, \text{vec}(\Phi)] \in \mathbb{R}^{210}$ be the vector consisting of $\boldsymbol{y}$ and the columns of Φ converted by 'vec' operator, there exists

$$\dot{\boldsymbol{z}} = \boldsymbol{G}(\boldsymbol{z}) \Rightarrow \begin{cases} \dot{\boldsymbol{y}} & = \boldsymbol{F}(y) \\ \text{vec}(\dot{\Phi}) & = \text{vec}(D_y \boldsymbol{F}\, \Phi) \end{cases} \tag{46}$$

The Φ matrix integrated from Eq. (45) maps states and costates along a given continuous trajectory. When the discontinuity is encountered at the switching time t_s, the STM compensation $\Psi(t_s)$ across the discontinuity should be determined. Suppose there are N discontinuities at $t_1,\ t_2, \cdots, t_N$, $\Phi(t_f, t_0)$ is calculated through the chain rule as

$$\Phi(t_f, t_0) = \Phi(t_f, t_N)\Psi(t_N)\Phi(t_N^-, t_{N-1}^+)\Psi(t_{N-1}) \cdots \Phi(t_2^-, t_1^+)\Psi(t_1)\Phi(t_1^-, t_0) \tag{47}$$

Suppose the discontinuity detected at t_s is indicated by a switching function S crossing a threshold η, there are two possible cases:

1) $S = S_\varepsilon$, $\varepsilon = 0$, $\eta = 0$ for the FO problem. In this case, $\boldsymbol{y}$ is continuous and $\dot{\boldsymbol{y}}$ is discontinuous. The discontinuity is conduced by the throttle switching function. Thrust throttle u jumps between 0 and 1 at t_s. $\Psi(t_s)$ is calculated as

$$\Psi(t_s) = \frac{\partial \boldsymbol{y}(t_s^+)}{\partial \boldsymbol{y}(t_s^-)} = I_{14\times 14} + \left(\dot{\boldsymbol{y}}(t_s^+) - \dot{\boldsymbol{y}}(t_s^-)\right) \frac{\partial S_\varepsilon}{\partial \boldsymbol{y}} / \dot{S}_\varepsilon \tag{48}$$

2) $S = S_d$, $u \neq 0$, $\eta = 0$ for both TO and EO2FO problems. In this case, both $\boldsymbol{y}$ and $\dot{\boldsymbol{y}}$ are discontinuous. The discontinuity is conduced by the shadow switching function. Thrust throttle u jumps between a non-zero value and 0 at t_s. $\Psi(t_s)$ is calculated as

$$\Psi(t_s) = \frac{\partial \boldsymbol{y}(t_s^+)}{\partial \boldsymbol{y}(t_s^-)} = I_{14\times 14} + \frac{\partial \Delta \boldsymbol{y}}{\partial \boldsymbol{y}} + \left(\dot{\boldsymbol{y}}(t_s^+) - \dot{\boldsymbol{y}}(t_s^-) - \dot{\Delta \boldsymbol{y}}\right) \frac{\partial S_d}{\partial \boldsymbol{y}} / \dot{S}_d \tag{49}$$

where $\Delta \boldsymbol{y} = [\mathbf{0}_{7\times 1},\ \Delta \boldsymbol{\lambda}_{\mathrm{mee}},\ 0]$ and its time derivative is

$$\dot{\Delta \boldsymbol{y}} = \frac{\partial \Delta \boldsymbol{y}}{\partial \boldsymbol{y}} \dot{\boldsymbol{y}}(t_s^-) + \frac{\partial \Delta \boldsymbol{y}}{\partial t} \tag{50}$$

Switching Detection Techniques

The switching detection technique is used to compute accurately the throttle and shadow switching time instants, which is essential in twofold. Firstly, the $\Psi(t_s)$ at the switching time t_s is indispensable for the accuracy of gradient computation. Secondly, the integration error accumulates across the discontinuity if the switching time is not explicitly detected. Consider a switching function S and the constant threshold η, the task is to find t_s such that $S(t_s) = \eta$. Suppose that at consecutive time instants t_k and t_{k+1}, there exists $(S_k - \eta) \times (S_{k+1} - \eta) < 0$, where $S_k \coloneqq S(t_k, \boldsymbol{y}(t_k))$ and $S_{k+1} \coloneqq S(t_{k+1}, \boldsymbol{y}(t_{k+1}))$, the switching detection is then implemented (refers to Zhang et al[7]). The switching detection method is embedded into the integration process, with the accuracy as 10^{-12}.

Remark 3 *It is assumed that the throttle switching time and shadow switching time do not coincide.*

Two-level Continuation

The ε continuation from EO solution to FO solution benefits to alleviate the difficulty to solve FO problem. However, the effect of shadow eclipse conduces the control and costate discontinuity, which narrows the convergence domain to solve TO and EO problems. In order to effectively find the solution, the another continuation level is designed to solve TO and EO problems.

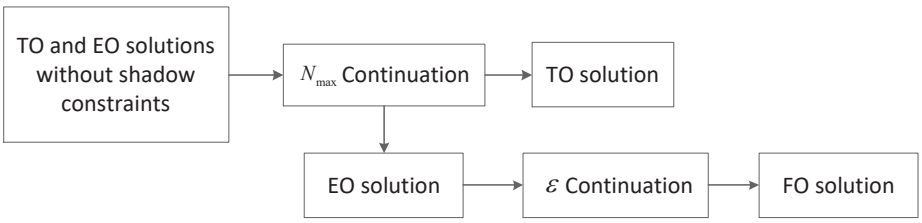

Figure 2: The continuation strategy.

Let N_s be the number of shadows that have been passed by the spacecraft, and $N_{\max}$ be the user-defined maximum number of shadows, the shadow is active only when $N_s \leq N_{\max}$. For the inactive shadow, it increases the N_s value, but the engine is not affected by the shadow. The idea is to find the low-thrust transfers without shadow constraints first. Then the continuation proceeds by gradually increasing $N_{\max}$, until $N_s = N_{\max}$ is true for the corresponding optimal trajectory. The two-level continuation strategy is shown in Fig. 2. The first level is $N_{\max}$ continuation to solve TO and EO problems, while the second level is ε continuation to solve FO problem.

Note that for the TO problem, the shooting method may fail using previous solution as initial guess to solve the TO problem with new $N_{\max}$, since the guess transfer time is not close to the new solution. In this case, the new initial guess with previous initial costate and increased transfer time is attempted to solve the problem. The guess transfer time is gradually increased until a new solution is found.

Integration flowchart

The integration flowchart presented in Zhang et al.[7] is insufficient to solve low-thrust transfers considering Earth-shadow eclipses. In this work, the flowchart is augmented to involve Earth-shadow related branches.

For simplicity of discussion, let $u_{\text{type}} = \{\text{'on', 'middle', 'off'}\}$ be the status of engine, the logic of which is

$$u_{\text{type}} = \begin{cases} \text{on}, & \text{if} \quad u = 1 \\ \text{middle}, & \text{if} \quad u \in (0,1) \\ \text{off}, & \text{if} \quad u = 0 \end{cases} \tag{51}$$

The augmented integration flowchart is presented in Fig. 3. The inputs required to execute one-step integration are 1) t_k, the kth time step; 2) h_p, the size of time step predicted by previous step of integration; 3) $\boldsymbol{z}_k$, the full 210-dimensional state; 4) u_{type}, the engine status at kth step; 5) N_s, the number of shadows that have been passed by the spacecraft; 6) p_{type}, defined in Eq. (16), labels the position of the spacecraft with respect to the shadow at kth step; 7) $\tilde{p}_{\text{type}}$, labels the position of the spacecraft with respect to the active shadow at kth step, defined as

$$\tilde{p}_{\text{type}} = \begin{cases} \text{in}, & \text{if} \quad S_d < 0 \quad \text{and} \quad \boldsymbol{r} \cdot \hat{\boldsymbol{s}} < 0 \quad \text{and} \quad N_s \leq N_{\max} \\ \text{out}, & \text{if} \quad \text{otherwise} \end{cases} \tag{52}$$

Thus $\tilde{p}_{\text{type}} = p_{\text{type}}$ if sufficiently large $N_{\max}$ value is adopted. Here, p_{type} is used to compute N_s, since $\tilde{p}_{\text{type}}$ fails to detect the inactive shadow. The command $N_s \leftarrow N_s + 0.5$ is implemented every time when p_{type} switches its value.

In Fig. 3, three branches separate at the beginning of integration according to u_{type}. For each integration block, a prediction on $\boldsymbol{z}_{k+1}$, i.e., $\boldsymbol{z}_{k+1} = \boldsymbol{\psi}_{\text{RK}}(\boldsymbol{z}_k, t_k, t_k + h_p, u_{\text{type}})$, is executed, using variable-step seventh/eighth-order Runge-Kutta integration scheme. Note that $\boldsymbol{z}_{k+1}$ is the state corresponding to $t_{k+1} = t_k + h_f$, where h_f is the corrected time step according to the integration accuracy which is set to 10^{-12} in the following.

For the u_{type} being 'on' or 'medium', the execution blocks are similar. Take u_{type} = 'on' as an example. The u_{type} = 'on' occurs only when $\tilde{p}_{\text{type}}$ = 'out'. Since the engine switches off when the active Earth's shadow is encountered, the first task after one-step integration prediction is to check the logic variable $\tilde{p}_{\text{type},k+1}$ at t_{k+1}, computed by Eq. (52). If $\tilde{p}_{\text{type},k+1}$ = 'out' is returned, the thrust throttle u is determined by the throttle switching function S_{k+1} ($S \coloneqq S_t$ for the TO problem and $S \coloneqq S_\varepsilon$ for the EO2FO problem) at t_{k+1}. The almost same execution block on the branch u_{type} = 'on' of the flowchart in Zhang et al.[7] is implemented. The slightly difference is when $S_{k+1} > \varepsilon$, simultaneously $\varepsilon \neq 0$. In this case, since the solution point is not saved, h_p is reduced and the switch of p_{type} is checked. If p_{type} is switched, then N_s is rollback as $N_s \leftarrow N_s - 0.5$ and p_{type} is rollback as the previous value.

Otherwise, if $\tilde{p}_{\text{type},k+1}$ = 'in' is returned, indicating that the spacecraft enters into the active shadow at t_{k+1}, it is then required to determine the shadow switching time t_s. Let S_c be the value of the throttle switching function S at t_s. If $S_c < -\varepsilon$, $\tilde{p}_{\text{type}}$ is updated to $\tilde{p}_{\text{type},k+1}$, STM is compensated using Eq. (49) and u_{type} is updated to 'off'. If $S_c \geq -\varepsilon$ which means that the switching indicated by throttle switching function S exists within $[t_k, t_{k+1}]$, h_p is reduced, simultaneously, N_s and p_{type} are rollback.

The most complex branch is the case when $u_{\text{type},k}$ = 'off'. The first task after one-step prediction is to check $\tilde{p}_{\text{type}}$. If $\tilde{p}_{\text{type}}$ = 'in' which indicates that the spacecraft locates inside the active shadow at $k$tk step, the next task is to check whether the spacecraft still locates inside the active shadow at t_{k+1}. If $\tilde{p}_{\text{type},k+1}$ = 'in', the spacecraft locates inside the shadow at t_{k+1} and the solution is saved. Otherwise, if $\tilde{p}_{\text{type},k+1}$ = 'out', it means the spacecraft flies out of the active shadow, then the detection of shadow switching time t_s is implemented. The $u(t_s^+)$ instantaneous after t_s is determined by the value of S_c. For example, if $S_c < -\varepsilon$, u_{type} is updated to 'on', $\tilde{p}_{\text{type}}$ is updated to $\tilde{p}_{\text{type},k+1}$, and STM compensation is calculated using Eq. (49).

If $\tilde{p}_{\text{type}}$ = 'out', it indicates that the spacecraft locates outside the active shadow and the engine switches off due to $S > \varepsilon$. If $\tilde{p}_{\text{type},k+1}$ = 'in' is returned, it means that the spacecraft flies inside the shadow at t_{k+1}. Thus the shadow switching time is detected. Since $\Delta u = 0$, there is no need to update STM, but the shadow status is updated if $S_c > \varepsilon$. Otherwise, if $\tilde{p}_{\text{type},k+1}$ = 'out' is returned, indicating that the Earth's shadow is not encountered at t_{k+1}, the almost same execution block on the branch u_{type} = 'off' of the flowchart in Zhang et al.[7] is implemented. The slightly difference when $S_{k+1} < -\varepsilon$ and $\varepsilon \neq 0$ is the rollback of N_s and p_{type}.

NUMERICAL SIMULATIONS

The GTO to GEO transfers are simulated as a case study. The physical constants are listed in Table 1, where LU is the Earth radius, $\text{VU} = \sqrt{\mu/\text{LU}}$ and $\text{TU} = \text{LU}/\text{VU}$. The initial and terminal orbital elements are listed in Table 2. Since the terminal inclination and eccentricity are both set to null, the definitions of Ω and w are invalid, thus they are set as free variables. Then the terminal conditions in Eq. (6) are determined by Eq. (1). Moreover, $m_0 = 100\,\text{kg}$, $I_{\text{sp}} = 3100\,\text{s}$, $T_{\max} = 0.5$ N and $\theta_{s,0} = 0\ \text{deg}$. All simulations are conducted under an Intel Core i7-9750H, CPU@2.6 GHz,

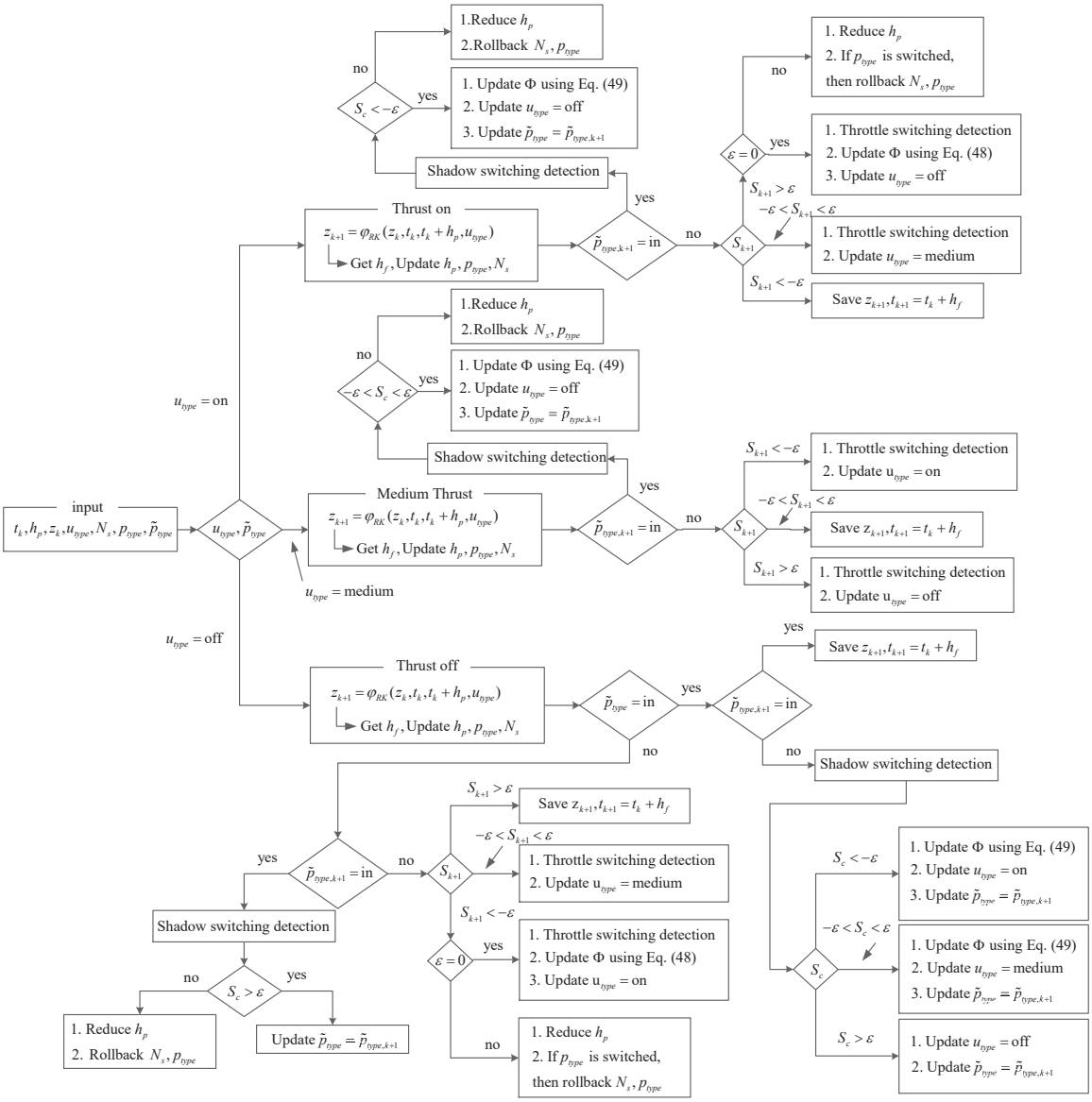

Figure 3: The generic integration scheme.

Windows 10 system with MATLAB R2019a.

Table 1: Physical constants.

Physical constant	Value
Earth gravitational constant, μ	$398600.4418\ \mathrm{km}^3/\mathrm{s}^2$
Gravitational field, g_0	$9.80665\ \mathrm{m}/\mathrm{s}^2$
Length unit, LU	$6378.1371\ \mathrm{km}$
Time unit, TU	$806.8111\ \mathrm{s}$
Velocity unit, VU	$7.9054\ \mathrm{km}/\mathrm{s}$
Mass unit, MU	$100\ \mathrm{kg}$
Earth diameter, D_p	2 LU
Sun diameter, D_s	1391020 km
Earth-Sun distance, $\delta_{p,s}$	1.4959787069×10^8 km

Table 2: Initial and terminal classical orbit elements.

Type	a [km]	e	i [deg]	Ω [deg]	w [deg]	θ [deg]
GTO	24505	0.725	7	0	0	0
GEO	42165	0	0	free	free	free

Table 3: The summary of simulation results.

Case	Type	$(\boldsymbol{\lambda}_0^*)^\top$	t_f [days]	m_f [kg]
1	TO w/o	$[-379.267601, -1283.576320, -0.141068, 369.000865, -17.577798, 1.177378, 768.997700]$	4.87	93.07
2	TO	$[-628.194423, -2412.755582, 30.900696, 403.082227, -414.850054, 2.807813, 1022.597380]$	5.82	92.60
3	EO w/o	$[-0.042555, -0.115290, 0.000081, 0.052083, -0.001659, 0.000043, 0.101126]$	6	93.77
4	EO	$[-0.060418, -0.066766, 0.004004, 0.112987, -0.043122, -0.000164, 0.209059]$	6	93.03
5	FO	$[-0.045632, -0.052496, 0.002768, 0.086850, -0.029471, -0.000127, 0.158596]$	6	93.15
6	EO 2ed	$[-0.062954, -0.062754, 0.004824, 0.117465, -0.059984, -0.000215, 0.231036]$	6	92.86
7	FO 2ed	$[-0.048712, -0.049306, 0.003429, 0.093393, -0.042355, -0.000174, 0.180451]$	6	92.95

The summary of numerical solutions is given in Table 3. With respect to the TO problem, the TO solution without shadow eclipses is reported as case 1 in Table 3, while the TO solution considering shadow eclipses is given as case 2 in Table 3. The total number of shadows that the spacecraft passes through for case 2 is 7. From cases 1–2, it can be seen that the transfer time of TO solution with shadow eclipses is longer than the one without shadow eclipses. At the same time, the corresponding fuel consumption of the former is more than the later. The TO trajectory of case 2 is shown in Figs. 4a. The TO variations of u, S_t and S_d are shown in Figs. 5a, where the red dash line is plotted to indicate the threshold of S_d. The variations of costate are shown in Fig. 6a where the shadow effect on the costate is apparent. The variations of a, e and i are shown as blue lines in Fig. 7.

The EO and FO solutions are summarized as cases 3–5 in Table 3, where the transfer time is set to 6 days. Again, the EO solutions without shadow, as case 3, is solved first by random guess. Through the two-level continuation, the EO and FO solutions are found, summarized as cases 4–5 in Table 3, respectively. For case 5, totally 9 shadows are passed through by the spacecraft. The FO

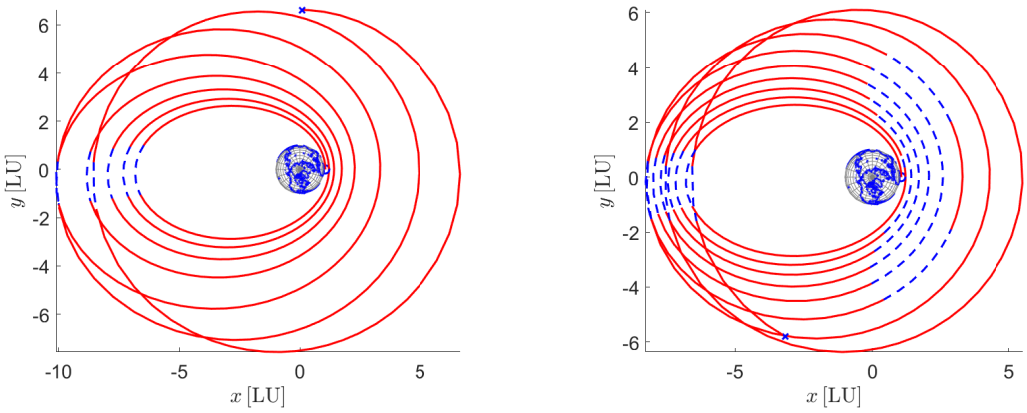

(a) Time-optimal trajectory.

(b) Fuel-optimal trajectory.

Figure 4: Time-optimal and fuel-optimal trajectories for cases 2 and 5 in Table 3, respectively.

trajectory for case 5 is shown in Figs. 4b, where the coast segments conduced by S_ε exist around perigee and the shadow region is around apogee. The FO variations of u, S_t and S_d are shown in Figs. 5b. The variations of costate is shown in Fig. 6b. The variations of a, e and i are shown as red dash lines in Fig. 7.

It is interesting that the EO and FO problems have multiple solutions. The second EO and FO solutions are reported as cases 6–7 in Table 3. The FO trajectory and the variations of u, S_ε and S_d are shown in Fig. 8. Compared with the solution obtained by Woollands and Taheri,[6] both FO trajectories pass through 8 times of the shadow, and the variations of u are coincide with each other. The final mass of FO solution obtained by Woollands and Taheri[6] is 93.08 kg, while our solution results in 92.95 kg. The mass difference is slightly different (0.13% w.r.t. m_0). Compared with the hyperbolic tangent smoothing method,[6] the explicit dependence of time on the shadow is considered in this work. Moreover, the solution with accurate bang-bang control can be obtained, without using approximation.

CONCLUSION

This work considers the low-thrust optimization in presence of Earth-shadow eclipses. The developed method incorporates analytic derivatives, switching detection technique, and two-level continuation with an augmented integration flowchart. The proposed continuation strategy enhances the algorithmic robustness and efficiency. The advantages of the proposed indirect method include that: 1) there is no need to prescribe the thrust structure a priori; 2) it enables to find accurate bang-bang solutions for both time-optimal and fuel-optimal problems; 3) it provides accurate gradients for robust convergence. Finally, the GTO to GEO transfers are simulated to test the algorithm performance.

ACKNOWLEDGMENT

Yang Wang acknowledges the support of this work by the China Scholarship Council (Grant no.201706290024).

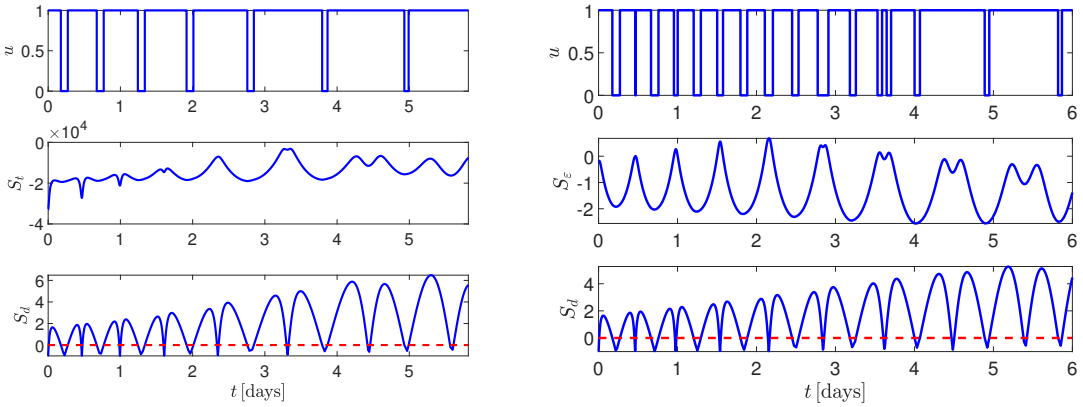

(a) Time-optimal u, S_t and S_d.

(b) Fuel-optimal u, S_ε and S_d.

Figure 5: Time-optimal (case 2) and fuel-optimal (case 5) variations of u, S_t, S_ε and S_d.

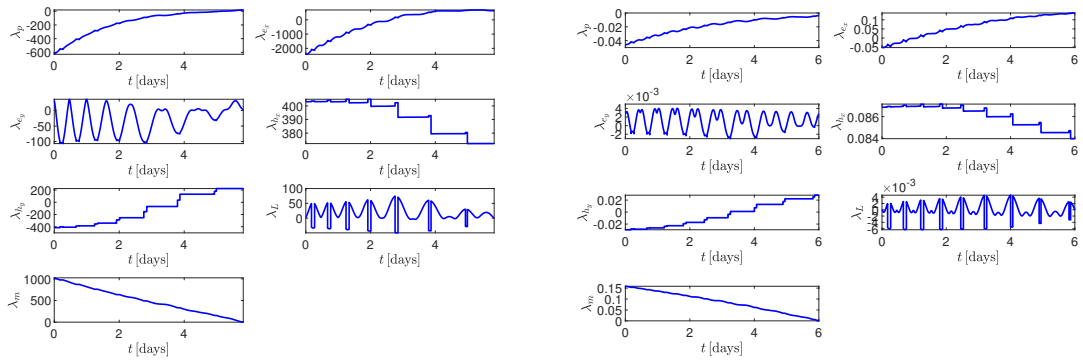

(a) Time-optimal costate variation.

(b) Fuel-optimal costate variation.

Figure 6: Time-optimal (case 2) and fuel-optimal (case 5) costate variations.

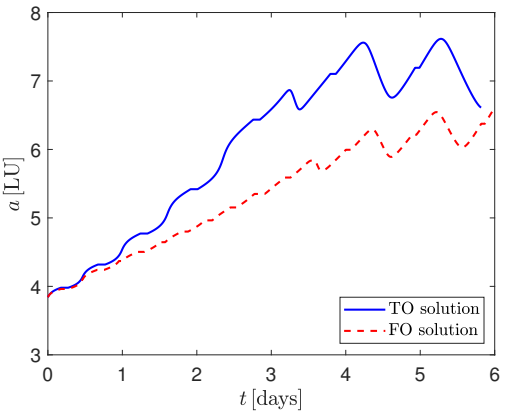

(a) Semi-major axis a

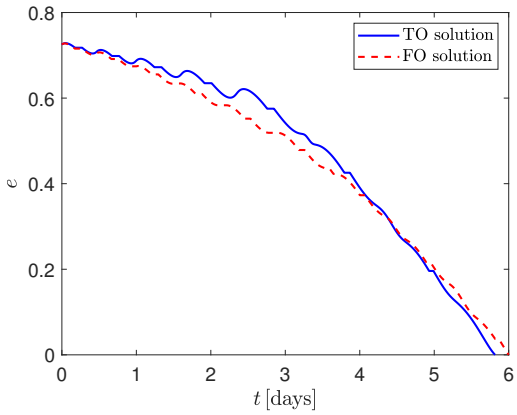

(b) Eccentricity e

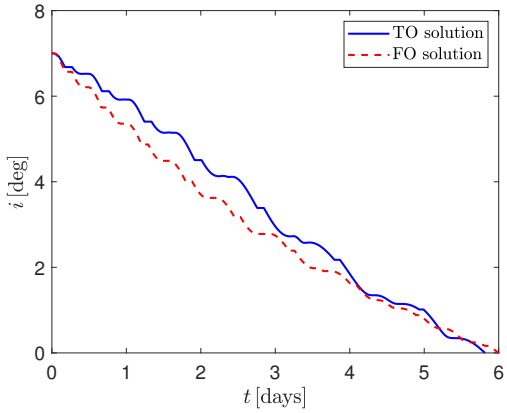

(c) Inclination i

Figure 7: Variations of a, e and i for cases 2 and 5 in Table 3.

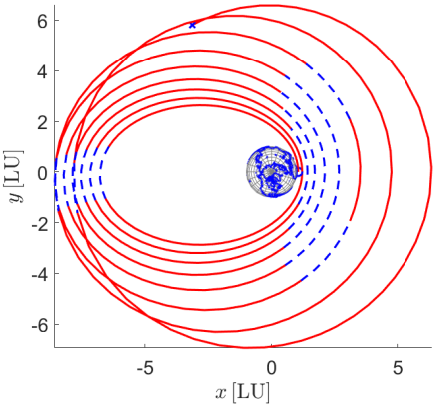

(a) Fuel-optimal trajectory.

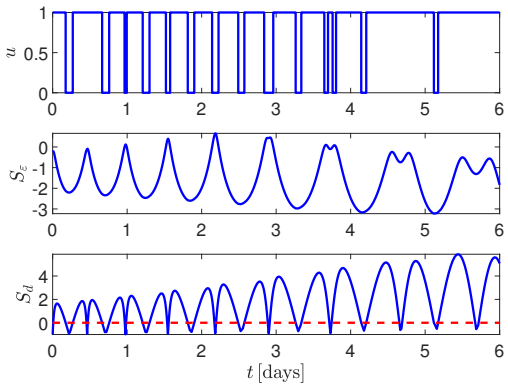

(b) Variations of u and S_ε and S_d.

Figure 8: Fuel-optimal trajectory and the corresponding variations of u and S_ε and S_d for the second solution (case 7).

REFERENCES

[1] A. V. Rao, "A Survey of Numerical Methods for Optimal Control," *Advances in the Astronautical Sciences*, Vol. 135, No. 1, 2009, pp. 497–528.

[2] A. E. Bryson and Y.-C. Ho, *Applied Optimal Control: Optimization, Estimation and Control*. Taylor and Francis, 1975, doi:10.1201/9781315137667.

[3] C. Ferrier and R. Epenoy, "Optimal Control for Engines with Electro-Ionic Propulsion under Constraint of Eclipse," *Acta Astronautica*, Vol. 48, No. 4, 2001, pp. 181–192, doi:10.1016/S0094-5765(00)00158-2.

[4] M. Cerf, "Fast Solution of Minimum-Time Low-Thrust Transfer with Eclipses," *Proceedings of the Institution of Mechanical Engineers, Part G: Journal of Aerospace Engineering*, Vol. 233, No. 7, 2019, pp. 2699–2714, doi:10.1177/0954410018785971.

[5] S. Geffroy and R. Epenoy, "Optimal Low-Thrust Transfers with Constraints—Generalization of Averaging Techniques," *Acta Astronautica*, Vol. 41, No. 3, 1997, pp. 133–149, doi:10.1016/S0094-5765(97)00208-7.

[6] R. Woollands and E. Taheri, "Optimal Low-Thrust Gravity Perturbed Orbit Transfers with Shadow Constraints," *The 2019 AAS/AIAA Astrodynamics Specialist Conference, Portland, Maine*, 2019.

[7] C. Zhang, F. Topputo, F. Bernelli-Zazzera, and Y.-S. Zhao, "Low-Thrust Minimum-Fuel Optimization in the Circular Restricted Three-Body Problem," *Journal of Guidance, Control, and Dynamics*, Vol. 38, No. 8, 2015, pp. 1501–1510, doi:10.2514/1.G001080.

[8] J. L. Junkins and E. Taheri, "Exploration of Alternative State Vector Choices for Low-Thrust Trajectory Optimization," *Journal of Guidance, Control, and Dynamics*, Vol. 42, No. 1, 2019, pp. 47–64, doi:10.2514/1.G003686.

[9] K. F. Graham and A. V. Rao, "Minimum-Time Trajectory Optimization of Low-Thrust Earth-Orbit Transfers with Eclipsing," *Journal of Spacecraft and Rockets*, Vol. 53, No. 2, 2016, pp. 289–303, doi:10.2514/1.A33416.

[10] J. T. Betts, "Optimal Low–Thrust Orbit Transfers with Eclipsing," *Optimal Control Applications and Methods*, Vol. 36, No. 2, 2015, pp. 218–240, doi:10.1002/oca.2111.